Vibro-acoustic simulation of damped orthotropic plates with the wave based method

H. Devriendt [1], **D. Vandepitte** [1], **W. Desmet** [1]
[1] KU Leuven, Department of Mechanical Engineering,
Celestijnenlaan 300 B, B-3001, Heverlee, Belgium
e-mail: **Hendrik.Devriendt@kuleuven.be**

Abstract
The wave based method was developed as an efficient methodology for the steady state simulation of vibro-acoustic systems. So far this method could only be used to predict the behaviour of simple panels made out of isotropic materials. With the current rise in importance of lightweight composite panels, there is increasing interest in the efficient simulation of panels with direction dependent properties and more complex damping behaviour. To address this need, in this paper, the application range of the wave-based method is expanded in two directions. In a first step the isotropic material model is extended towards an orthotropic one. Second, a versatile damping model, based on the Augmented Hooke's Law, is integrated into the methodology. Next, the method is applied to three cases. The first one consists of a rectangular composite panel that is excited by a distributed load. In the second case, a vibro-acoustic model is studied by coupling the panel to an acoustic cavity with a simple geometry. Lastly, a model is made of an existing vibro-acoustic test setup on which the composite panel is mounted. Results are compared to a FEM reference model.

1 Introduction

Due to the increased demand for products with a higher energy efficiency, the transport industry relies more and more on the use of lightweight materials to lower the weight of their products. These are often composite materials like honeycomb panels and fibre reinforced polymers. Due to their complex structure, their properties are no longer isotropic and they show frequency dependent damping. This makes it more challenging to predict and optimise their vibro-acoustic behaviour. In order to perform this in a time and cost efficient manner, design engineers increasingly call on CAE techniques. These lower the need for costly physical prototypes and allow for optimisations in the early product development stages.

Nowadays, element based methods like the Finite Element Method (FEM) [1] and the Boundary Element Method (BEM) [2], are the most common CEA techniques. They divide the problem domain into many small elements and use simple polynomial functions to approximate the solution in each element. The downside of this approach is that, as the frequency increases, an increasing number of elements is needed to obtain an accurate solution [3]. This limits their application range to low frequencies. The introduction of a frequency dependent damping model further lowers the applicability of the FEM. Since the FEM matrices become complex and frequency dependent, they are harder to solve with traditional solvers and modal reduction techniques become less applicable. This makes the method less suited for the simulation of composite lightweight panels.

A recently developed alternative to the element based methods is the Wave Based Method (WBM) [4, 5]. This deterministic simulation technique is based on an indirect Trefftz approach [6] and approximates the solution as a weighted sum of wave functions, which are exact solutions of the governing differential equation,

without the need to divide the domain into small elements. Due to these properties, the WBM has a high computational efficiency that allows it to tackle vibro-acoustic problems up into the mid-frequency region [7]. Until now, those models were limited to isotropic panels with simple damping behaviour. Since the WBM matrices are frequency dependent and complex, it has the potential for efficiently simulating complex materials with frequency dependent damping.

The goal of this contribution is to explore this potential through the development of the WBM for orthotropic plates and the implementation of a general damping model, based on the Augmented Hooke's Law [8]. The paper is structured as follows. Section 2 starts with a definition of the vibro-acoustic problem under study. A third section describes the numerical modelling techniques that are developed to solve this problem. In section 4, the method is applied to a number of case studies to assess its performance. A fifth section ends the paper with some concluding remarks.

2 Problem definition

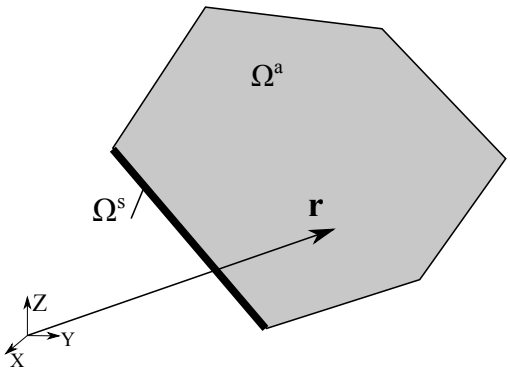

Figure 1: 3D vibro-acoustic problem.

The problem under study is a bounded 3D vibro-acoustic system, as depicted in Figure 1. The fluid inside the acoustic cavity Ω^a is characterised by mass density ρ_a and speed of sound c. It is assumed that this fluid shows linear, inviscid and adiabatic behaviour. The steady-state acoustic pressure $p(\mathbf{r})$ inside the cavity can then be described by the inhomogeneous Helmholtz equation [9]:

$$\Delta^2 p(\mathbf{r}) + k_a^2 p(\mathbf{r}) = Q_a, \qquad \mathbf{r} \in \Omega^a \tag{1}$$

where Δ^2 is the Laplacian operator, k_a the acoustic wave number, and Q_a a source term. The acoustic wave number is determined by the expression $k_a = \frac{\omega}{c}$, with ω the angular frequency under study. In order to have a unique solution to the problem, one boundary condition needs to be applied in each point of the boundary. This can be an acoustic boundary condition or a coupling condition that couples the acoustic pressure in the cavity to the displacements of the structural domain. The most common acoustic boundary conditions are:

- *pressure boundary condition*

$$R_p(\mathbf{r}) = p(\mathbf{r}) - \bar{p}(\mathbf{r}) = 0 \tag{2}$$

- *normal velocity boundary condition*

$$R_v(\mathbf{r}) = \mathcal{L}_v(p(\mathbf{r})) - \bar{v}_n(\mathbf{r}) = 0 \tag{3}$$

- *normal impedance boundary condition*

$$R_z(\mathbf{r}) = \mathcal{L}_v(p(\mathbf{r})) - \frac{p(\mathbf{r})}{\bar{Z}({}_n\mathbf{r})} = 0 \tag{4}$$

with $R_\bullet(\mathbf{r})$ the boundary residual and $\bar{p}(\mathbf{r})$, $\bar{v}_n(\mathbf{r})$ and $\bar{Z}({}_n\mathbf{r})$ the prescribed pressure, normal velocity and normal impedance respectively. $\mathcal{L}_v(\bullet)$ is the normal velocity operator.

The structural domain Ω^s consists of a thin orthotropic plate, whose steady-state transversal displacement w is governed by the orthotropic Kirchhoff equation [10]:

$$D_{11}\frac{\delta^4 w(\mathbf{r})}{\delta x^4} + 2(D_{12}+2D_{66})\frac{\delta^4 w(\mathbf{r})}{\delta x^2 y^2} + D_{22}\frac{\delta^4 w(\mathbf{r})}{\delta y^4} - k_b^4 w(\mathbf{r}) = P(\mathbf{r}), \qquad \mathbf{r}\ \epsilon\ \Omega^s \tag{5}$$

with D_{ij} the orthotropic plate parameters, k_b the structural wave number, and $P(\mathbf{r})$ a force excitation term. The structural wave number is equal to $\sqrt[4]{\omega^2\rho_s h}$, with ρ_s and h the mass density and thickness of the plate respectively. The expressions for the orthotropic plate parameters D_{ij} depend on the material parameters and on the adopted damping model. In this paper, a complex damping model based on the Augmented Hooke's Law (AHL) [8, 11, 12, 13] is used. This is discussed in detail in section 3.2, where also the expressions for D_{ij} are derived. Since (5) is a fourth order partial differential equation, two boundary conditions are required at each point of the boundary. Typical boundary conditions are:

- *kinematic boundary conditions*: prescribed displacement and rotation (clamped edge)

$$\begin{aligned} R_w(\mathbf{r}) &= w(\mathbf{r}) - \bar{w}(\mathbf{r}) = 0 \\ R_{\theta_n}(\mathbf{r}) &= \mathcal{L}_{\theta_n}(w(\mathbf{r})) - \bar{\theta}_n(\mathbf{r}) = 0 \end{aligned} \tag{6}$$

- *mixed boundary conditions*: prescribed displacement and bending moment (simply supported edge)

$$\begin{aligned} R_w(\mathbf{r}) &= w(\mathbf{r}) - \bar{w}(\mathbf{r}) = 0 \\ R_{m_n}(\mathbf{r}) &= \mathcal{L}_{m_n}(w(\mathbf{r})) - \bar{m}_n(\mathbf{r}) = 0 \end{aligned} \tag{7}$$

with $R_\bullet(\mathbf{r})$ the boundary residual and $\bar{w}(\mathbf{r})$, $\bar{\theta}_n(\mathbf{r})$ and $\bar{m}_n(\mathbf{r})$ the prescribed displacement, normal rotation and normal bending moment respectively. $\mathcal{L}_{\theta_n}(\bullet)$ and $\mathcal{L}_{m_n}(\bullet)$ are the normal rotation and normal bending moment operators respectively. The coupling with the acoustic domain is realised through the force excitation term since the dynamic pressure in the cavity acts as an excitation over the whole surface of the plate.

3 Modelling techniques

To find a solution to this vibro-acoustic problem, the Wave Based Method (WBM) is used to numerically model both the acoustic and the structural domain. An extension to the WBM had to be developed to allow the method to simulate orthotropic plates. A first section presents the modelling procedure of the WBM for vibro-acoustic problems, with focus on the extension to orthotropic plates. To allow the method to simulate complex damping behaviour, a damping model based on the AHL is developed in a second section.

3.1 The Wave Based Method (WBM)

The Wave Based Method (WBM) is a deterministic simulation technique, based on an indirect Trefftz approach [6]. This means that the method includes knowledge of the problem in the base functions for the field variables [14]. Desmet [4] originally developed the method for isotropic Kirchhoff plates and for 3D interior acoustic problems that are governed by the Helmholtz equation. Further research extended the applicability of the method to other problems such as in-plane vibrating plates [15] and poro-elastic materials [16, 17]. [5] gives a more complete overview of the current capabilities of the WBM.

Until now, only isotropic materials could be tackled with the WBM for plates. In this paper, the method is extended to enable the simulation of the transverse vibration of thin orthotropic plates. In the next paragraphs, the four steps of the numerical modelling procedure of the WBM are explained, applied to an orthotropic vibro-acoustic model. The focus is on the specific adaptations to include the orthotropic material behaviour and on the coupling of the orthotropic plate to the acoustic cavity.

Step 1: Partitioning into convex subdomains
Desmet [4] showed that, to ensure that the method converges to the exact solution of the problem, convexity of the considered domain is a sufficient condition. When the problem geometry has a non-convex shape, a first step in the modelling procedure is to divide the domain into non-overlapping convex subdomains. To ensure continuity of the field variables over the interfaces between adjacent subdomains, continuity conditions will be applied to both subdomains.

Step 2: Field variable expansion for each subdomain
In each of the subdomains, the dynamic variables $u(\mathbf{r})$ (either pressure p or displacement w) are approximated by a solution expansion $\hat{u}(\mathbf{r})$ of wave functions $\Phi_i(\mathbf{r})$, supplemented with particular solution functions $u_{p,j}(\mathbf{r})$:

$$u(\mathbf{r}) \approx \hat{u}(\mathbf{r}) = \sum_i \Phi_i(\mathbf{r}) w_i + \sum_j \hat{u}_{p,j}(\mathbf{r}) \tag{8}$$

The unknown degrees of freedom are the weights w_i of each wave function. In accordance to the Trefftz approach, these wave functions are chosen such that they exactly satisfy the governing differential equation. This way, no errors are made on the domain equations. This contrasts with the finite element method, where the field variables are described in terms of simple, often linear, shape functions that approximate the solution by taking enough elements per wavelength.

For 3D acoustic domains, Desmet [4] proposed the following set of wave functions:

$$\begin{cases} \Phi_r(\mathbf{r}) = cos(k_{r,x}x)cos(k_{r,y}y)e^{-jk_{r,z}z} & r = 0, 1, ..., n_r \\ \Phi_s(\mathbf{r}) = cos(k_{s,x}x)e^{-jk_{s,y}y}cos(k_{s,z}z) & s = 0, 1, ..., n_s \\ \Phi_t(\mathbf{r}) = e^{-jk_{t,x}x}cos(k_{t,y}y)cos(k_{t,z}z) & t = 0, 1, ..., n_t \end{cases} \tag{9}$$

In order for these functions to be exact solutions to the Helmholtz equation, the wave number components in the three directions, $k_{i,x}, k_{i,y}$ and $k_{i,x} (i = r, s, t)$, need to satisfy:

$$k_{r,x}^2 + k_{r,y}^2 + k_{r,z}^2 = k_{s,x}^2 + k_{s,y}^2 + k_{s,z}^2 = k_{t,x}^2 + k_{t,y}^2 + k_{t,z}^2 = k_a^2 \tag{10}$$

Since an infinite series of wave numbers can satisfy this equation, a truncation strategy is used to select a finite set. This is done based on the dimensions L_x x L_y x L_z of the smallest rectangular bounding box enclosing the domain. For each of the wave functions, two of the three wave number components are chosen such that an integer number of half wavelengths equals the dimension of the bounding box in the corresponding direction. The third wave number is then calculated to satisfy relation (10):

$$\begin{cases} (k_{r,x}, k_{r,y}, k_{r,z}) = (\frac{a_1\pi}{L_x}, \frac{a_2\pi}{L_y}, \pm\sqrt{k_a^2 - (\frac{a_1\pi}{L_x})^2 - (\frac{a_2\pi}{L_y})^2}) \\ (k_{s,x}, k_{s,y}, k_{s,z}) = (\frac{a_3\pi}{L_x}, \pm\sqrt{k_a^2 - (\frac{a_3\pi}{L_x})^2 - (\frac{a_4\pi}{L_z})^2}, \frac{a_4\pi}{L_z}) \\ (k_{t,x}, k_{t,y}, k_{t,z}) = (\pm\sqrt{k_a^2 - (\frac{a_5\pi}{L_y})^2 - (\frac{a_6\pi}{L_z})^2}, \frac{a_5\pi}{L_y}, \frac{a_6\pi}{L_z}) \end{cases} \tag{11}$$

with $a_i \in \{0, 1, 2, ..., n_i\} (i = 1, 2, 3, 4, 5, 6)$ This infinite series is truncated by the user by selecting a value for the truncation parameter T:

$$\frac{n_1}{L_x} \approx \frac{n_2}{L_y} \approx \frac{n_3}{L_x} \approx \frac{n_4}{L_z} \approx \frac{n_5}{L_y} \approx \frac{n_6}{L_z} \leq T\frac{k_a}{\pi} \tag{12}$$

If n_p acoustic point sources are present in the domain, for each of them a particular solution function is added to the expansion (8). This particular solution represents the free field pressure field generated by an acoustic monopole at location $(x_{p,j}, y_{p,j}, z_{p,j})$:

$$\hat{p}_{p,j}(\mathbf{r}) = \frac{j\rho_a\omega q}{4\pi}\frac{e^{-jk_a\mathbf{r_{p,j}}}}{\mathbf{r_{p,j}}}, \qquad j = 1, 2, ..., n_p \tag{13}$$

with $\mathbf{r_{p,j}} = \sqrt{(x-x_{p,j})^2+(y-y_{p,j})^2+(z-z_{p,j})^2}$, j the imaginary unit and q the source strength.

For structural domains, a similar set of wave functions exist, that this time satisfy the isotropic Kirchoff plate equation. However, since an orthotropic thin plate is described by a different partial differential equation than an isotropic one, these wave functions need to be modified. The shape of the functions can be kept the same as for isotropic plates:

$$\begin{cases} \Phi_{b1}(\mathbf{r}) = cos(k_{b1,x}x)e^{-jk_{b1,y}y} & b_1 = 0,1,...,n_{b1} \\ \Phi_{b2}(\mathbf{r}) = e^{-jk_{b2,x}x}cos(k_{b2,y}y) & b_2 = 0,1,...,n_{b1} \end{cases} \tag{14}$$

Substituting these functions into the orthotropic plate equation (5), yields the following constraints for the wave number components $k_{b1,x}$, $k_{b1,y}$, $k_{b2,x}$ and $k_{b2,y}$:

$$\begin{array}{l} D_{11}k_{b1,x}^4 + 2(D_{12}+2D_{66})k_{b1,x}^2k_{b1,y}^2 + D_{22}k_{b1,y}^4 = k_b^4 \\ D_{11}k_{b2,x}^4 + 2(D_{12}+2D_{66})k_{b2,x}^2k_{b2,y}^2 + D_{22}k_{b2,y}^4 = k_b^4 \end{array} \tag{15}$$

Again, a finite set of wave number components has to be selected out of the infinite set that can satisfy this constraint. Following the same strategy as for the acoustic problem, based on the dimensions L_x x L_y of the smallest rectangle that can enclose the domain, a selection is made:

$$k_{b1,x} = \frac{b_1\pi}{L_x} \quad k_{b1,y} = \begin{cases} \pm\sqrt{\frac{\sqrt{D_{22}k_b^4+((D_{12}+2D_{66})^2-D_{11}D_{22})k_{b1,x}^4}-(D_{12}+2D_{66})k_{b1,x}^2}{D_{22}}} \\ \pm j\sqrt{\frac{\sqrt{D_{22}k_b^4+((D_{12}+2D_{66})^2-D_{11}D_{22})k_{b1,x}^4}+(D_{12}+2D_{66})k_{b1,x}^2}{D_{22}}} \end{cases} \tag{16}$$

$$k_{b2,y} = \frac{b_2\pi}{L_y} \quad k_{b2,x} = \begin{cases} \pm\sqrt{\frac{\sqrt{D_{22}k_b^4+((D_{12}+2D_{66})^2-D_{11}D_{22})k_{b2,y}^4}-(D_{12}+2D_{66})k_{b2,y}^2}{D_{11}}} \\ \pm j\sqrt{\frac{\sqrt{D_{22}k_b^4+((D_{12}+2D_{66})^2-D_{11}D_{22})k_{b2,y}^4}+(D_{12}+2D_{66})k_{b2,y}^2}{D_{11}}} \end{cases} \tag{17}$$

with $b_i \in \{0,1,2,...,n_{bi}\}(i=1,2)$. This infinite series is truncated by selecting a value for the truncation parameter T:

$$\frac{n_{b1}\sqrt[4]{D_{11}}}{L_x} \approx \frac{n_{b2}\sqrt[4]{D_{22}}}{L_y} \leq T\frac{k_b}{\pi} \tag{18}$$

When a force is applied to the structural domain, one or more particular solution functions need to be added to expansion (8). In the case of a point force, a particular solution function is used that represents the displacement field generated by a point force applied to an infinite plate. This particular function can be found by using the Green's functions. When the plate is coupled with an acoustic domain, the pressure inside the cavity acts as the force excitation on the plate. For this type of load, a particular solution in an explicit form can be found because the wave functions that are used to describe the pressure field, have the same shape as the structural wave functions. For each acoustic wave function, a particular solution is added to the expansion of the displacement (8). For simplicity, it is assumed that the structural domain lies in the xy-plane such that the z-component of the acoustic wave functions (9) at the surface of the plate is zero. For each of the three types of acoustic wave functions (Φ_r, Φ_s and Φ_t), a particular solution ($\Phi_{r,p}$, $\Phi_{s,p}$ and $\Phi_{t,p}$ respectively) can be found by assuming that it has the same shape as the acoustic wave function, with an unknown scaling factor b_i:

$$\begin{array}{l} \Phi_{r,p}(\mathbf{r}) = b_1cos(k_{r,x}x)cos(k_{r,y}y) \\ \Phi_{s,p}(\mathbf{r}) = b_2cos(k_{s,x}x)e^{-jk_{s,y}y} \\ \Phi_{t,p}(\mathbf{r}) = b_3e^{-jk_{t,x}x}cos(k_{t,y}y) \end{array} \tag{19}$$

Substituting the displacement $w(\mathbf{r})$ and the force $P(\mathbf{r})$ in equation (5) with these particular solution functions and the acoustic excitation functions respectively, yields a solution for b_1, b_2 and b_3:

$$\begin{array}{l} b_1 = \frac{1}{D_{11}k_{r,x}^4+2(D_{12}+2D_{66})k_{r,x}^2k_{r,y}^2+D_{22}k_{r,y}^4-k_b^4} \\ b_2 = \frac{1}{D_{11}k_{s,x}^4+2(D_{12}+2D_{66})k_{s,x}^2k_{s,y}^2+D_{22}k_{s,y}^4-k_b^4} \\ b_3 = \frac{1}{D_{11}k_{t,x}^4+2(D_{12}+2D_{66})k_{t,x}^2k_{t,y}^2+D_{22}k_{t,y}^4-k_b^4} \end{array} \tag{20}$$

Note that the existence of a particular solution for every force distribution of the form $cos \cdot cos$ or $cos \cdot exp$ means that any kind of distributed load, that can be decomposed into a series of these functions with different wave numbers, can be simulated.

Step 3: Construction of the system matrices
Due to the choice of wave functions, the solution expansion (8) inherently satisfies the governing domain equation, independent of the values of the degrees of freedom. The boundary and continuity conditions between different domains, however, are not automatically satisfied. To minimize these errors, a weighted residual approach is used where the residuals on the boundary are orthogonalised with respect to a set of weighting functions $t_k(\mathbf{r})$. Every boundary and continuity condition can then be written as a weighted residual term $\mathcal{R}_k$:

$$\mathcal{R}_k = \int_{\Gamma_k} \mathcal{D}_k(t_k(\mathbf{r}))R_k(\mathbf{r}) = 0, \quad k = 1, 2, ..., n_k \tag{21}$$

with Γ_k the boundary on which the condition is applied, n_k the total number of boundary and continuity conditions, and $\mathcal{D}_k$ a differential operator that orthogonalises $t_k(\mathbf{r})$ to the boundary residual $R_k(\mathbf{r})$, like the ones described in equations (2) to (4), (6) and (7). Similar to a Galerkin weighted approach, that is often applied in the finite element method, the same function expansion is used for the weighting functions $t_k(\mathbf{r})$ as for the field variables (8):

$$t_k(\mathbf{r}) = \sum_i \Phi_{k,i}(\mathbf{r})\tilde{t}_i \tag{22}$$

with $\Phi_{k,i}$ the wave functions of the field variable expansion present in the corresponding $R_k(\mathbf{r})$ from equation (21). Summation of all the weighted residual terms $\mathcal{R}_k$ and substitution of expansions (8) and (22) into these residuals leads to a matrix system of equations of the form:

$$[\mathbf{A}]\{\mathbf{u}\} = \mathbf{b} \tag{23}$$

with $\mathbf{A}$ the system matrix, $\mathbf{u}$ a vector containing all the unknown wave function contribution factors w_i from expansion (8) and $\mathbf{b}$ the right-hand side vector that results from non-zero boundary conditions and excitations that require particular solution functions. [4] provides a more detailed explanation of how this matrix system is constructed.

Step 4: Solving the system of equations and post-processing
In a final step, the matrix system of equations (23) is solved for the unknown contribution factors of the wave functions. These contribution factors are then substituted in equation (8) to obtain an analytical expression for the approximate field variable $\hat{u}(\mathbf{r})$. Derivative quantities such as acoustic velocity and structural stresses can be calculated without loss of spatial precision by applying differential operators to the wave function sets.

3.2 Augmented Hooke's Law (AHL)

The current structural WBM for plates has limited capabilities to include damping in the model. Only proportional damping is readily supported. To allow the simulation of more complex materials, a more general damping model is developed, based on the Augmented Hooke's Law in the frequency domain [8]. The AHL is a 3D, completely general constitutive material model that has a convenient formulation in the frequency domain. Dovstam originally developed the method for isotropic materials. Dalenbring [18] later applied the concepts of AHL to obtain a transverse isotropic material damping model. In this paper, the method is further extended to an orthotropic AHL based damping model.

The Augmented Hooke's Law replaces the stiffness matrix $\mathbf{H}$, that relates the stresses σ to the strains ε, with an augmented constitutive matrix $\hat{\mathbf{H}}$:

$$\sigma = \hat{\mathbf{H}}(\omega)\varepsilon \tag{24}$$

For a 3D material model, the stresses and strains consist of six components and $\hat{\mathbf{H}}(\omega)$ is a six by six matrix. It is formulated by the AHL as a combination of the classic elastic constitutive matrix and an augmentation matrix $\mathbf{H}_\Delta(\omega)$, that incorporates the damping.

$$\hat{\mathbf{H}}(\omega) = \mathbf{H} + \mathbf{H}_\Delta(\omega) \tag{25}$$

with

For an orthotropic material, the stiffness matrix $\mathbf{H}$ is determined by nine parameters: three Young's moduli (E_x, E_y and E_z), three Poisson's ratios (ν_{xy}, ν_{yz} and ν_{zx}) and three shear moduli (G_{xy}, G_{yz} and G_{zx}). This allows $\mathbf{H}$ to be expanded into nine terms:

$$\mathbf{H} = h_{11}\mathbf{H}_{11} + h_{22}\mathbf{H}_{22} + h_{33}\mathbf{H}_{33} + h_{44}\mathbf{H}_{44} + h_{55}\mathbf{H}_{55} + h_{66}\mathbf{H}_{66} + h_{12}\mathbf{H}_{12} + h_{13}\mathbf{H}_{13} + h_{23}\mathbf{H}_{23} \tag{26}$$

where h_{ij} are factors containing the nine constitutive parameters and H_{ij} are constant matrices that are independent of the constitutive parameters. The expressions for h_{ij} and H_{ij} can be found in Appendix A.

The augmentation matrix $\mathbf{H}_\Delta(\omega)$ is defined by the AHL as:

$$\mathbf{H}_\Delta(\omega) = \sum_{l=1}^{N_l} \frac{j\omega}{j\omega + \beta_l} \mathbf{F}_l \mathbf{G}_l^{-1} \mathbf{F}_l \tag{27}$$

with β_l the relaxation frequencies, F_l the coupling matrices and G_l the real dissipation matrices. For an orthotropic material, each F_l is defined as:

$$\mathbf{F}_l = f_{1,l}\mathbf{H}_{11} + f_{2,l}\mathbf{H}_{22} + f_{3,l}\mathbf{H}_{33} + f_{4,l}\mathbf{H}_{44} + f_{5,l}\mathbf{H}_{55} + f_{6,l}\mathbf{H}_{66} + f_{7,l}\mathbf{H}_{12} + f_{8,l}\mathbf{H}_{13} + f_{9,l}\mathbf{H}_{23} \tag{28}$$

where $f_{i,l}$ are material damping parameters and H_{ij} are the same as in equation (26). Each dissipation matrix G_l is defined as:

$$G_l = \alpha_l \begin{bmatrix} 1 & 0 & 0 & 0 & 0 & 0 \\ 0 & 1 & 0 & 0 & 0 & 0 \\ 0 & 0 & 1 & 0 & 0 & 0 \\ 0 & 0 & 0 & \frac{1}{2} & 0 & 0 \\ 0 & 0 & 0 & 0 & \frac{1}{2} & 0 \\ 0 & 0 & 0 & 0 & 0 & \frac{1}{2} \end{bmatrix} \tag{29}$$

with α_l another AHL damping parameter.

Based on the orthotropic AHL constitutive model, expressions for the orthotropic plate parameters $D_{i,j}$ in equation (5) can be derived. Since the Kirchhoff plate theory considers thin plates, it assumes that the stresses in the thickness direction of the plate (σ_{zz}, τ_{xz} and τ_{yz}) are zero. This is known as the plane stress situation. To impose this assumption, the inverse S (the compliance matrix) of the augmented stiffness matrix $\hat{\mathbf{H}}(\omega)$ is calculated:

$$\mathbf{S}(\omega) = \hat{\mathbf{H}}^{-1}(\omega) \quad \rightarrow \quad \varepsilon = \mathbf{S}(\omega)\sigma \tag{30}$$

The plane stress condition can then be imposed by removing the rows and columns from S that correspond to σ_{zz}, τ_{xz} and τ_{yz}. Taking the inverse of the resulting three by three compliance matrix, transforms it back into the stiffness form. The orthotropic plate parameters $D_{i,j}$ can then be calculated by multiplying this three by three stiffness matrix with $\frac{h^3}{12}$, with h the plate thickness.

4 Case studies

The WBM for damped orthotropic plates is verified through three application cases. The first one consists of an orthotropic panel that's excited by a distributed load. The second and third cases are vibro-acoustic systems that are excited by an acoustic point source. The former couples the panel to a cavity of simple geometry. The latter system is an existing vibro-acoustic test set-up on which the panel is mounted.

The results are verified by comparing them to those obtained with the FEM. The FEM models are constructed and solved with the commercial package Comsol 4.3a. This software, however, only supports elements based on the Reissner-Mindlin plate theory while the WBM is based on the Kirchhoff plate theory. Cremer et al. [19] showed that the differences between the two plate theories are negligible when the thickness of the plate is at least six times smaller than the smallest bending wave under consideration. This condition is satisfied in the frequency range of interest for all of the studied cases.

The WBM routines are implemented in Matlab r2012a. All the calculations are performed on a 64-bit windows system with a 2.6GHz dual core Ivy Bridge processor and 8GB of RAM.

4.1 Case 1: Panel under distributed loading

4.1.1 Model description

The panel is a rectangle of size A2 (0.42m x 0.594m) and has a thickness of 0.5mm. The material properties are listed in table 1. The regular constitutive parameters correspond to a unidirectional fibre reinforced polymer. For the damping model, only one term is used for the augmentation matrix $\mathbf{H}_\Delta(\omega)$ (27). The damping parameters are analogue to those used by Dovstam [8] and Lesieutre [20]. They are not necessarily realistic damping parameters for the considered material but are chosen to illustrate the capabilities of the method. The panel is clamped on all four edges and excited through a distributed load of shape $cos(K_x x) \cdot cos(K_y y)$. The wave numbers K_x and K_y are chosen such that the wavelengths of the excitation are one third of the corresponding dimension of the panel.

E_x	$120 \cdot 10^9\,\mathrm{Pa}$	$f_{1,1}$	$4.77 \cdot 10^6\,\mathrm{N/m^2}$
E_y	$10 \cdot 10^9\,\mathrm{Pa}$	$f_{2,1}$	$4.77 \cdot 10^6\,\mathrm{N/m^2}$
E_z	$10 \cdot 10^9\,\mathrm{Pa}$	$f_{3,1}$	$4.77 \cdot 10^6\,\mathrm{N/m^2}$
ν_{xy}	0.3	$f_{4,1}$	$0\,\mathrm{N/m^2}$
ν_{yz}	0.3	$f_{5,1}$	$0\,\mathrm{N/m^2}$
ν_{zx}	0.3	$f_{6,1}$	$0\,\mathrm{N/m^2}$
G_{xy}	$4.9 \cdot 10^9\,\mathrm{Pa}$	$f_{7,1}$	$4.77 \cdot 10^6\,\mathrm{N/m^2}$
G_{yz}	$4.9 \cdot 10^9\,\mathrm{Pa}$	$f_{8,1}$	$4.77 \cdot 10^6\,\mathrm{N/m^2}$
G_{zx}	$4.9 \cdot 10^9\,\mathrm{Pa}$	$f_{9,1}$	$4.77 \cdot 10^6\,\mathrm{N/m^2}$
ρ_s	$1510\,\mathrm{kg/m^3}$	α_1	$8 \cdot 10^3\,\mathrm{N/m^2}$
		β_1	$8 \cdot 10^3\,\mathrm{rad/s}$

Table 1: Material properties of the panel

4.1.2 Results

Figure 2 shows the frequency response of the panel, evaluated at a quarter of the width and length of the panel, compared to the FEM reference solution. The WBM solution is calculated with truncation factor 4, resulting in 380 wave functions being used at the highest frequency. The FEM reference model uses 10 quadratic elements per wavelength, totalling 5632 elements for the whole panel. The results show a good match between the models. To highlight the effect of the introduced damping model, the response of the undamped system is shown as well.

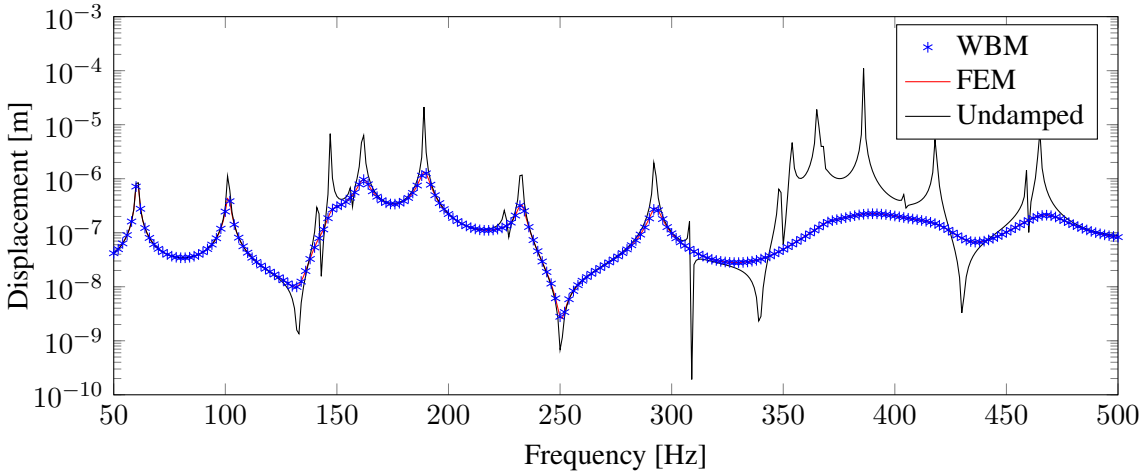

Figure 2: Displacement of the damped and undamped panel for case 1.

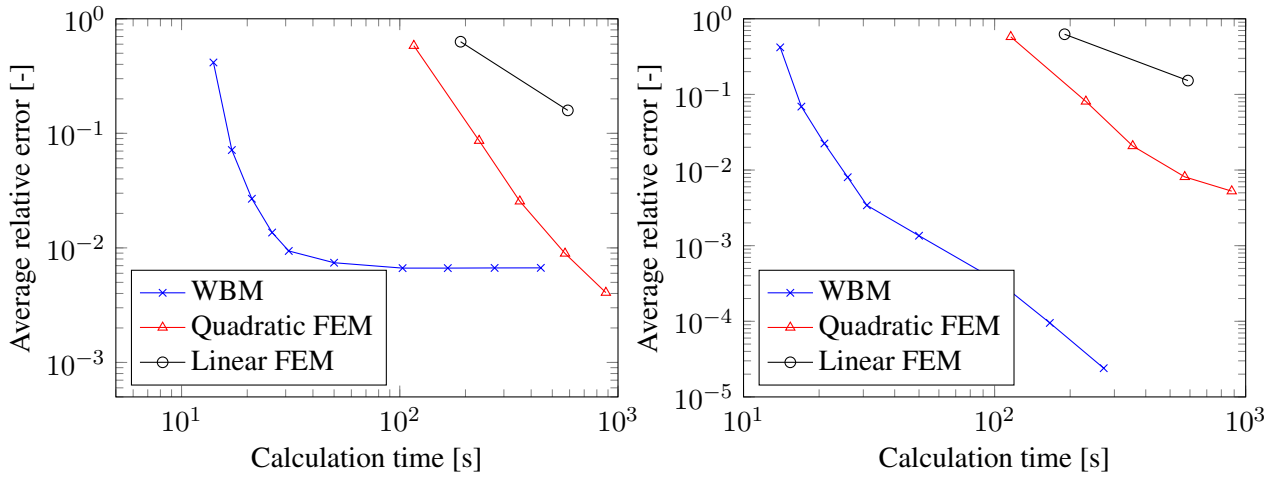

(a) FEM as reference.

(b) WBM as reference.

Figure 3: Relative error as function of calculation time.

To further investigate the accuracy and efficiency of the method, a convergence study is performed. The response of the panel is calculated for different values of the truncation parameter and is evaluated in two points: one at a quarter of the width and length, and one in the middle of the panel. Next, the relative error is calculated with the FEM as a reference and this error is averaged over the frequency and over the two evaluation points. Plotting these averaged errors against the calculation time shows the convergence behaviour. For comparison, the convergence of the FEM is calculated as well by changing the number of elements and by using different discretisation techniques. The results in figure 3a show the superior convergence behaviour of the WBM. The relative error of the WBM saturates at about 10^{-2}. This indicates that the accuracy of the WBM surpasses that of the FEM reference model. This suspicion is confirmed when the finest WBM model, with truncation factor 6, is used as a reference, see Figure 3b. Now none of the method's accuracies stagnate and the keep converging towards the finest WBM result. The figures also show that to achieve the same accuracy as a quadratic FEM model, the WBM only needs a calculation time that's a full order of magnitude smaller. This is even more remarkable considering that the FEM model uses an optimised commercial solver while the WBM runs as a research code in Matlab. The reason why the FEM struggles to produce accurate results, is the damping model that introduces complex numbers in the FEM matrices, making them more difficult to solve. This is not an issue for the WBM since its matrices are always complex.

4.2 Case 2: Vibro-acoustic model of simple geometry

4.2.1 Model description

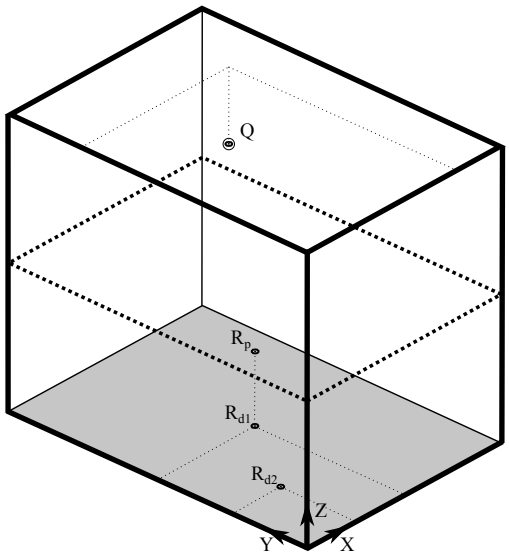

Figure 4: Geometry for case 2. Point Q indicates the location of the acoustic monopole source. The solution is post-processed in points $R_\bullet$. The dashed lines indicate boundaries of the different WBM domains.

The problem geometry for case 2 is shown in figure 4. A rigid wall cavity with a height of 0.5m is added on top of the panel from case 1. The air in the cavity is characterised by a density of $1.225\,\mathrm{kg/m^3}$ and a speed of sound of $340\,\mathrm{m/s}$. The system is excited by an acoustic monopole, located in the point Q (0.3150m, 0.4455m, 0.3750m), and the panel is clamped on all four edges. The WBM model consist of one structural domain for the panel and two acoustic domains. The cavity is split into two domains such that the panel and the acoustic source are not in the same domain. This is necessary since there are no particular solution functions available to couple the acoustic particular solution of the monopole source to the panel.

4.2.2 Results

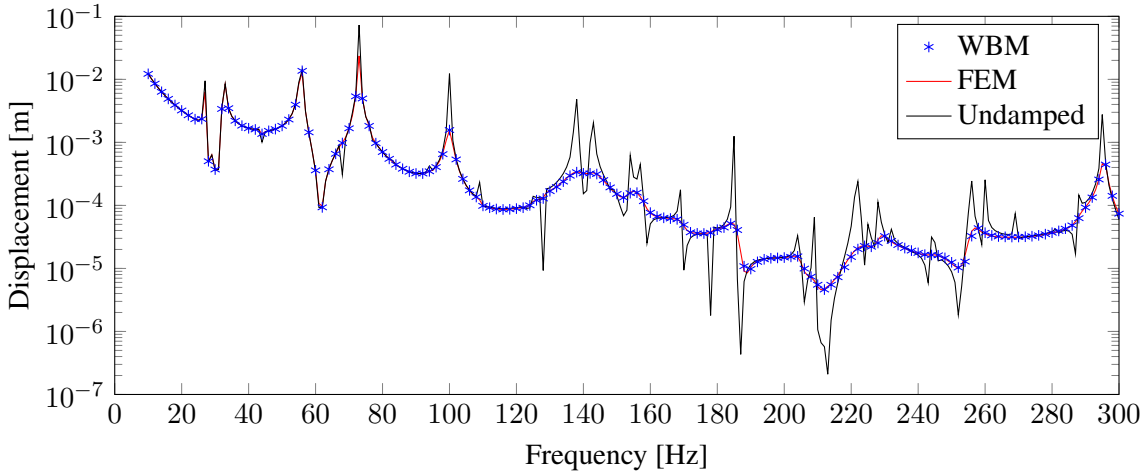

Figure 5: Displacement of the damped and undamped panel for case 2.

Figure 5 shows the displacement of the panel, evaluated in the same point as the one from figure 2. The WBM solution is calculated with truncation factor 5, resulting in 1758 wave functions being used at the highest frequency. The FEM reference model consists of 158682 quadratic elements. The results show that, also for this vibro-acoustic case, there is a good match between the models.

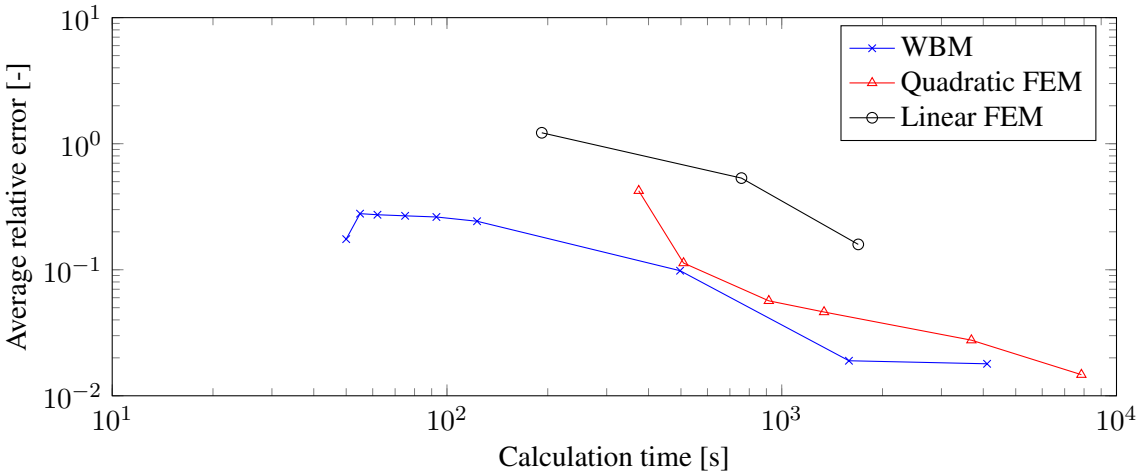

Figure 6: Relative error as function of calculation time.

The accuracy and efficiency is again further assessed through a convergence study. A FEM model that uses 15 quadratic elements per wavelength is used as the reference solution. The results in figure 6 show that the WBM still converges faster than the FEM but the difference is less pronounced than in case 1. This is caused by the multiple WBM domains that are needed for this model. Since the calculation of the boundary residuals is the most computationally expensive part of the WBM, the higher number of domains and thus boundaries is, the lower the overall efficiency is.

4.3 Case 3: Vibro-acoustic model of an existing test set-up

4.3.1 Model description

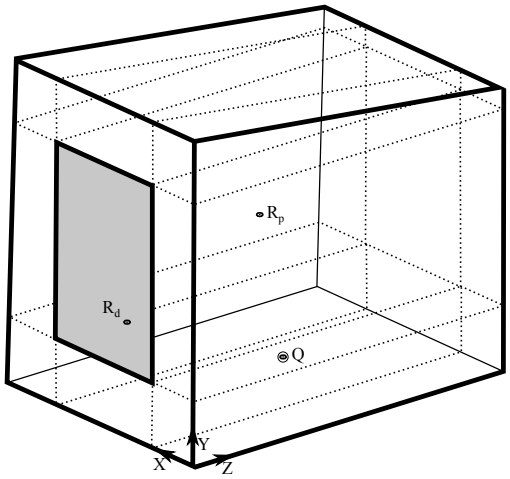

Figure 7: Geometry of the test set-up. Point Q indicates the location of the acoustic monopole source. The solution is post-processed in points $R_\bullet$. The dashed lines indicate boundaries of the different WBM domains.

The test set-up consists of a convex cavity (1.122m x 0.82m x 0.982m) with non-parallel walls, on which the panel from case 1 is mounted (figure 7). An acoustic monopole source is located at point Q (0.29m, 0.099m, 0.561m). The walls of the cavity are considered rigid and the panel is clamped on all its edges. Although the cavity is convex, it still needs to be partitioned in 9 subdomains, such that the panel is a complete boundary of only one subdomain. The WBM model thus consists of 9 acoustic domains and one structural domain.

4.3.2 Results

The goal of this case is to show that the WBM can handle real world applications and provide results that are within engineering precision. As such, a detailed convergence study is not performed on this model. Figure 8 shows the displacement of the panel at a quarter of the width and length of the panel. The WBM solutions is calculated with truncation factor 4, resulting in 2274 wave functions being used at the highest frequency. The FEM reference model consists of 115491 quadratic elements. There is good agreement between the WBM solution and the FEM reference, with accuracy being within engineering precision. The calculation time for the WBM model, however, is only on third of that of the FEM reference. If this test set-up would be used for optimising the vibro-acoustic performance of a panel, the WBM has an additional benefit aside from the already higher convergence rate than the FEM. Since only the panel changes, the boundary residuals of the acoustic domains do not need to be recomputed between different iterations. This drastically reduces the computational times since the calculation of these residuals is the most demanding.

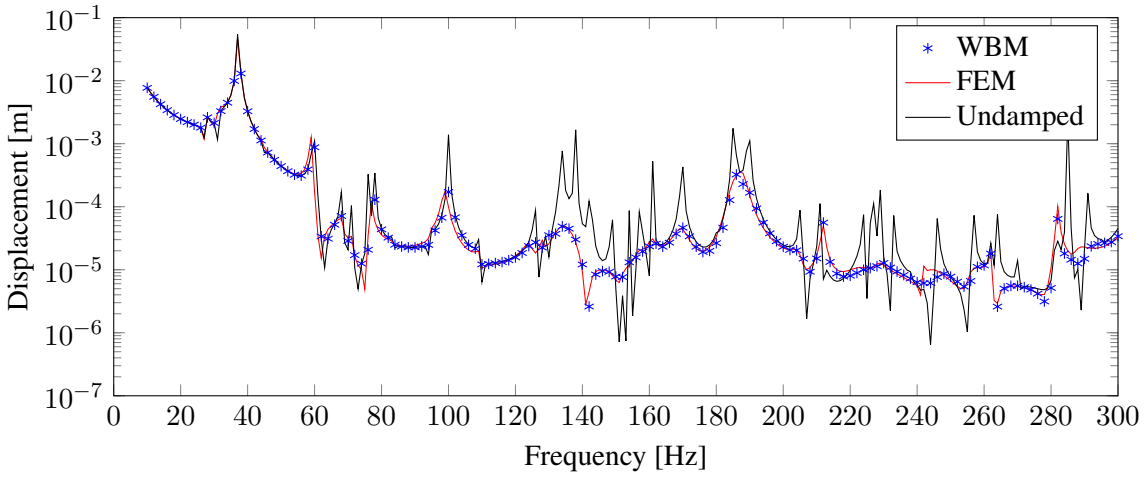

Figure 8: Displacement of the damped and undamped panel for case 3.

5 Conclusion

Efficient prediction of the vibro-acoustic behaviour of composite lightweight panels is becoming more and more important. These panels are often characterised by orthotropic material properties and frequency dependent damping behaviour, making them challenging to solve with traditional element based techniques. To address this need, in this paper, the WBM for orthotropic plates was developed and a general damping model, based on the Augmented Hooke's Law, was added.

The method was verified in three case studies trough comparison with the FEM. Results of the first two cases showed that the WBM has a faster convergence rate and an overall higher efficiency than the FEM, at least for simple geometries. A third case demonstrated the capability of the method to model a real life example, in the form of an existing vibro-acoustic test set-up.

Future research will further study the efficiency of the method for geometrically more complex cases. The possibility of a hybrid WBM-FEM approach being superior in some cases will also be investigated. The high efficiency of the method also suggest that it is a useful technique for optimisation, an application that might be explored in the future.

Acknowledgements

The research of Hendrik Devriendt is funded by a PhD grant of the Institute for the Promotion of Innovation through Science and Technology in Flanders (IWT-Vlaanderen). The Fund for Scientific Research Flanders (F.W.O.) and the Research Fund KU Leuven are also gratefully acknowledged for their support.

References

[1] O. C. Zienkiewicz, R. L. Taylor, *The Finite Element Method*, Vol. 1: the basis, Elsevier/Butterworth Heinemann, sixth Ed. (2005).

[2] P. Banerjee, R. Butterfield, *Boundary Element Methods in Engineering Science*, McGraw-Hill Book Company (1981).

[3] T. Lodygowski, W. Sumelka, *Limitations in application of finite element method in acoustic numerical simulation*, Journal of theoretical and applied mechanics, Vol. 44, (2006), pp. 849–865.

[4] W. Desmet, *A wave based prediction technique for coupled vibro-acoustic analysis*, Ph.D. thesis, KULeuven, division PMA (1998).

[5] E. Deckers, O. Atak, L. Coox, R. DAmico, H. Devriendt, S. Jonckheere, K. Koo, B. Pluymers, D. Vandepitte, W. Desmet, *The wave based method: An overview of 15 years of research*, Wave Motion, Vol. 51, (2014), pp. 550–565.

[6] E. Trefftz, *Ein gegenstück zum ritzschen verfahren*, *Proceedings of the 2nd International Congress on Applied Mechanics*, 131–137.

[7] W. Desmet, B. Pluymers, O. Atak, B. Bergen, E. Deckers, J. Huijssen, B. V. Genechten, K. Vergote, D. Vandepitte, *Simulation techniques for mid-frequency: vibro-acoustic virtual tools for real problems*, *Proceedings of the 20th Spring conference of the Korean Society of Noise and Vibration (KSNVE2010)*.

[8] K. Dovstam, *Augmented hooke's law in frequency domain: a three dimensional material damping formulation*, International Journal of Solids and Structures, Vol. 32, No. 19, (1995), pp. 2835–2852.

[9] P. Morse, K. Ingard, *Theoretical acoustics*, McGraw-Hill, New York (United States of America) (1968).

[10] S. Lekhnitskii, *Anisotropic plates*, Gordon and Breach (1968).

[11] M. Dalenbring, *Damping function estimation based on measured vibration frequency responses and finite-element displacement modes*, Mechanical Systems and Signal Processing, Vol. 13, No. 4, (1999), pp. 547–569.

[12] K. Dovstam, *Receptance model based on isotropic damping functions and elastic displacement modes*, International Journal of Solids and Structures, Vol. 34, No. 21, (1997), pp. 2733–2754.

[13] K. Dovstam, *Simulation of damped vibrations based on augmented hooke's law and elastic modes of vibration*, International Journal of Solids and Structures, Vol. 37, (2000), pp. 5413–5445.

[14] B. Pluymers, B. van Hal, D. Vandepitte, W. Desmet, *Trefftz-based methods for time-harmonic acoustics*, Archives of Computational Methods in Engineering (ARCME), Vol. 14, No. 4, (2007), pp. 343–381.

[15] C. Vanmaele, K. Vergote, W. Desmet, D. Vandepitte, *Simulation of in-plane vibrations of 2d structural solids with singularities using an efficient wave based prediction technique*, Computer Assisted Mechanics and Engineering Sciences, Vol. 19, (2012), pp. 135–171.

[16] E. Deckers, N.-E. Hörlin, D. Vandepitte, W. Desmet, *A wave based method for the efficient solution of the 2d poroelastic biot equations*, Computer Methods in Applied Mechanics and Engineering, Vol. 201-204, (2012), pp. 245–265.

[17] E. Deckers, D. Vandepitte, W. Desmet, *A wave based method for the axisymmetric dynamic analysis of acoustic and poroelastic problems*, Computer Methods in Applied Mechanics and Engineering, Vol. 257, (2013), pp. 1–16.

[18] M. Dalenbring, *An explicit formulation of a three-dimensional material damping model with transverse isotropy*, International Journal of Solids and Strucutres, Vol. 39, (2002), pp. 225–249.

[19] L. Cremer, M. Heckl, E. E. Ungar, *Structure-borne Sound: structural vibrations and sound radiation at audio frequencies*, Springer-Verlag, Berlin (1973).

[20] G. A. Lesieutre, *Finite element modelling of frequency-dependent material damping using augmenting thermodynamic fields*, Ph.D. thesis, University of California, Los Angeles.

A Appendix A: Detailed expansion of the orthotropic constitutive matrix

Hooke's law defines the orthotropic stiffness matrix $\mathbf{H}$ for a 3D material as:

$$\sigma = \mathbf{H}\varepsilon \tag{31}$$

with σ the stress vector and ε the strain vector:

$$\sigma = \begin{Bmatrix} \sigma_{xx} \\ \sigma_{yy} \\ \sigma_{zz} \\ \tau_{yz} \\ \tau_{zx} \\ \tau_{xy} \end{Bmatrix} \qquad \varepsilon = \begin{Bmatrix} \varepsilon_{xx} \\ \varepsilon_{yy} \\ \varepsilon_{zz} \\ \gamma_{yz} \\ \gamma_{zx} \\ \gamma_{xy} \end{Bmatrix} \tag{32}$$

The stiffness matrix can be decomposed in nine terms:

$$\mathbf{H} = h_{11}\mathbf{H}_{11} + h_{22}\mathbf{H}_{22} + h_{33}\mathbf{H}_{33} + h_{44}\mathbf{H}_{44} + h_{55}\mathbf{H}_{55} + h_{66}\mathbf{H}_{66} + h_{12}\mathbf{H}_{12} + h_{13}\mathbf{H}_{13} + h_{23}\mathbf{H}_{23} \tag{33}$$

The factors h_{ij} are:

$$h_{11} = \frac{(1 - \nu_{yz}\nu_{zy})}{(E_y E_z \Delta)} \qquad h_{22} = \frac{(1 - \nu_{zx}\nu_{xz})}{(E_z E_x \Delta)} \qquad h_{33} = \frac{(1 - \nu_{xy}\nu_{yx})}{(E_x E_y \Delta)} \tag{34}$$

$$h_{44} = G_{yz} \qquad h_{55} = G_{zx} \qquad h_{66} = G_{xy} \tag{35}$$

$$h_{12} = \frac{(\nu_{yx} + \nu_{zx}\nu_{yz})}{(E_y E_z \Delta)} \qquad h_{13} = \frac{(\nu_{zx} + \nu_{yx}\nu_{zy})}{(E_y E_z \Delta)} \qquad h_{23} = \frac{(\nu_{zy} + \nu_{zx}\nu_{xy})}{(E_z E_x \Delta)} \tag{36}$$

with

$$\Delta = \frac{(1 - \nu_{xy}\nu_{yx} - \nu_{yz}\nu_{zy} - \nu_{zx}\nu_{xz} - 2\nu_{xy}\nu_{yz}\nu_{zx})}{(E_x E_y E_z)} \tag{37}$$

and E_i the Young's moduli, G_{ij} the shear moduli and ν_{ij} the Poisson doefficients. The constant matrices H_{ij} are:

$$H_{11} = \begin{bmatrix} 1 & 0 & 0 & 0 & 0 & 0 \\ 0 & 0 & 0 & 0 & 0 & 0 \\ 0 & 0 & 0 & 0 & 0 & 0 \\ 0 & 0 & 0 & 0 & 0 & 0 \\ 0 & 0 & 0 & 0 & 0 & 0 \\ 0 & 0 & 0 & 0 & 0 & 0 \end{bmatrix} \quad H_{22} = \begin{bmatrix} 0 & 0 & 0 & 0 & 0 & 0 \\ 0 & 1 & 0 & 0 & 0 & 0 \\ 0 & 0 & 0 & 0 & 0 & 0 \\ 0 & 0 & 0 & 0 & 0 & 0 \\ 0 & 0 & 0 & 0 & 0 & 0 \\ 0 & 0 & 0 & 0 & 0 & 0 \end{bmatrix} \quad H_{33} = \begin{bmatrix} 0 & 0 & 0 & 0 & 0 & 0 \\ 0 & 0 & 0 & 0 & 0 & 0 \\ 0 & 0 & 1 & 0 & 0 & 0 \\ 0 & 0 & 0 & 0 & 0 & 0 \\ 0 & 0 & 0 & 0 & 0 & 0 \\ 0 & 0 & 0 & 0 & 0 & 0 \end{bmatrix} \tag{38}$$

$$H_{44} = \begin{bmatrix} 0 & 0 & 0 & 0 & 0 & 0 \\ 0 & 0 & 0 & 0 & 0 & 0 \\ 0 & 0 & 0 & 0 & 0 & 0 \\ 0 & 0 & 0 & 1 & 0 & 0 \\ 0 & 0 & 0 & 0 & 0 & 0 \\ 0 & 0 & 0 & 0 & 0 & 0 \end{bmatrix} \quad H_{55} = \begin{bmatrix} 0 & 0 & 0 & 0 & 0 & 0 \\ 0 & 0 & 0 & 0 & 0 & 0 \\ 0 & 0 & 0 & 0 & 0 & 0 \\ 0 & 0 & 0 & 0 & 0 & 0 \\ 0 & 0 & 0 & 0 & 1 & 0 \\ 0 & 0 & 0 & 0 & 0 & 0 \end{bmatrix} \quad H_{66} = \begin{bmatrix} 0 & 0 & 0 & 0 & 0 & 0 \\ 0 & 0 & 0 & 0 & 0 & 0 \\ 0 & 0 & 0 & 0 & 0 & 0 \\ 0 & 0 & 0 & 0 & 0 & 0 \\ 0 & 0 & 0 & 0 & 0 & 0 \\ 0 & 0 & 0 & 0 & 0 & 1 \end{bmatrix} \tag{39}$$

$$H_{12} = \begin{bmatrix} 0 & 1 & 0 & 0 & 0 & 0 \\ 1 & 0 & 0 & 0 & 0 & 0 \\ 0 & 0 & 0 & 0 & 0 & 0 \\ 0 & 0 & 0 & 0 & 0 & 0 \\ 0 & 0 & 0 & 0 & 0 & 0 \\ 0 & 0 & 0 & 0 & 0 & 0 \end{bmatrix} \quad H_{13} = \begin{bmatrix} 0 & 0 & 1 & 0 & 0 & 0 \\ 0 & 0 & 0 & 0 & 0 & 0 \\ 1 & 0 & 0 & 0 & 0 & 0 \\ 0 & 0 & 0 & 0 & 0 & 0 \\ 0 & 0 & 0 & 0 & 0 & 0 \\ 0 & 0 & 0 & 0 & 0 & 0 \end{bmatrix} \quad H_{23} = \begin{bmatrix} 0 & 0 & 0 & 0 & 0 & 0 \\ 0 & 0 & 1 & 0 & 0 & 0 \\ 0 & 1 & 0 & 0 & 0 & 0 \\ 0 & 0 & 0 & 0 & 0 & 0 \\ 0 & 0 & 0 & 0 & 0 & 0 \\ 0 & 0 & 0 & 0 & 0 & 0 \end{bmatrix} \tag{40}$$